APPLICATION OF ITERATIVE AIRBORNE LIDAR INVERSION AND ITS INTERPRETATION BY MEANS OF ECMWF OPERATIONAL ANALYSES

Iwona S. Stachlewska [1]* and Andreas Dörnbrack[2]

[1] *Alfred-Wegener-Institute for Polar and Marine Research, D-14473 Potsdam, Germany*
** now at Leosphere, EcolePolytechnique, 91128 Palaiseau Cedex,France, istachlewska@leosphere.fr*
[2] *Institut für Physik der Atmosphäre, DLR Oberpfaffenhofen, 82230 Wessling, Germany*

ABSTRACT

The iterative airborne lidar inversion scheme [1], based on the Klett's approach [2] but using for the calibration of the backscatter ratio profiles the measured signals itself, i.e. by determining an approximate near-field boundary value used as a constraint for the retrieval initiated in the far-field, is proposed and demonstrated. The method was applied to the data obtained with the short-range nadir-aiming Airborne Mobile Aerosol Lidar (AMALi) [3] during Foehn-like meteorological event lasting from 18 until 23 May 2004 during the Arctic Study of Tropospheric Clouds and Radiation (ASTAR) [4] campaign on Svalbard. Prevailing, nearly stationary easterly tropospheric winds past Svalbard formed on its west side a cloud-free area due to the adiabatic warming of the descending air parcels on the leeside of the mountains. In contrast to the Alpine Foehn events, the flow around Svalbard formed so-called corner-winds at the northern and southern tip of the islands. Associated with them characteristic triangular structures in the retrieved backscatter ratio profiles are discussed in terms of the outputs of the ECMWF operational analysis.

1. INTRODUCTION

The range corrected signal S of an nadir-aiming airborne lidar flying at altitude h_f reads:

$$S(h) = P(h)(h_f - h)^2 = C\beta(h)T^2_{[h_f,h]}(h)$$

$$T(h) = exp\,(-\int_{h_i}^{h} \alpha(\tilde{h})d\tilde{h})$$

where P denotes the mean number of detected photons, C the lidar instrumental constant, β the backscatter coefficient and T the transmission term dependent on α the extinction coefficient.

To solve this equation with respect to β and α usually the Klett's inversion [2] is used with assumption of the lidar ratio $LR=\alpha/\beta$ and calibration value far from the lidar β_{ref}. This method can be especially valuable for the short-range nadir-aiming airborne lidar data inversion measuring in the lower troposphere due to the high signal-to-noise ratio (S/N) of the obtained signals and due to the increase of aerosol loads with increase of each range-step.

On the other hand in this case (unlike for the long-range zenith-looking lidar) the largest term of the error propagation of the backscatter coefficient profiles is due to the wrong assumption of the backscatter calibration value (large $\delta\beta/\delta h$), while the wrong assumption of the lidar ratio contributes much less to the backscatter ratio uncertainty (small $\delta\beta/\delta LR$).

Hence, the main problem of using the Klett's approach arises from the difficulty of providing a calibration values for airborne profiles. For near-ground/sea troposphere, usually rich in turbulent aerosol generated by surface winds, the backscatter coefficient is highly variable during the flight and very difficult to guess. As difficult is to provide any reference backscatter value in the low troposphere due to the usual lack of aerosol free layers between the flight altitude and ground/sea level.

One of the ways to provide β_{ref} is in-situ onboard calibration (value at flight altitude and/or profiles by aircraft's descents). However, such lidar and in-situ measurements do not cover the same area and the aircraft itself greatly disturbs the measured atmosphere.

More intricate way to provide the calibration value can be achieved by use of the scanning lidar. Nadir to zenith flip of the laser beam allows to set the calibration value at any aerosol free layer above aircraft and to glue both signals at the flight altitude. However, such approach may result in problems due to the doubling of the lidar geometrical compression range. By horizontal scan the calibration value or profile can be obtained using the slope method [2], though only when assumption of the atmospheric homogeneity at flight altitude can be made.

As the realisations of mentioned ideas get tricky in a real life; costly (additional in-situ instrumentation), design challenging (laser beam flipper, space and energy consumption limitation in the aircraft), and time consuming (aircraft authorities certification), an easy alternative approach is needed.

2. METHODOLOGY, RESULTS AND ERRORS

Consider airborne lidar which geometrical compression is completed just after first few hundred meters from the system. If h_{gc} denote the altitude directly below such geometrical compression, then the attenuation of the emitted laser light along this path is negligible:

$$T_{[h_f,h_{gc}]} \approx 1 - (h_f - h_{gc}) \cdot \alpha(h_f) \lesssim 1$$

By neglecting the transmittance term and for known lidar constant C the backscatter at the altitude h_{gc} can be estimated for each time step during the flight:

$$\beta(h_{gc}) \gtrsim \frac{S(h_{gc})}{C}$$

The knowledge of $\beta(h_{gc})$ for all times during the flight allows application of the Klett's method with following constraint: the β_{ref} (backscatter coefficient calibration value chosen near the ground) must be set in a way, that the backscatter coefficient at the height h_{gc} calculated using the Klett's inversion matches the estimated value $\beta(h_{gc})$. Such calculation for each profile can be done using a simple Newton iterative approach and repeated for each time step along flight.

The method was applied to the data obtained with the AMALi onboard Polar 2 for two flights during distinct Foehn-like meteorological event lasting from 18 until 23 May 2004 during ASTAR campaign on Svalbard.

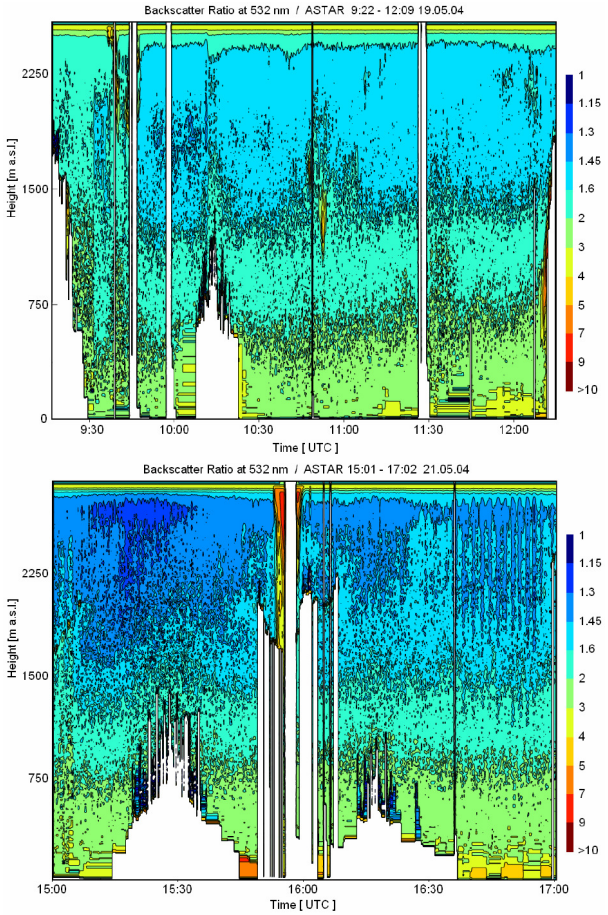

Fig.1 Calibrated backscatter ratio profiles along the flight retrieved using the iterative approach for 19 and 21 May 2004 during the ASTAR campaign. Note the characteristic triangular shape of aerosol/cloud distribution corresponding to the northern most leg of the flight path (Fig.3). Such aerosol shape on the 19 May is related to the vertically lifted isentropic surfaces (Fig.4, top) indicating enhanced vertical transport of the sea salt aerosols.

The backscatter ratio profiles were calculated using the AMALi's lidar constant $C=1.43\pm0.1\cdot10^{13}$ mVm^3sr [5]. The 15s temporal resolution corresponding to 1km spatial resolution was chosen to provide appropriate resolution for comparison with the ECMWF operational analyses (compare Sect.4). In the case of thick clouds the backscatter ratio could not be retrieved due to multiple scattering. The striking feature captured on both backscatter ratio plots (Fig.1) are triangularly-shaped aerosol gradients measured in the NW offshore Svalbard. In both cases, the flight paths were nearly parallel to these aerosol gradients (Fig.3).

For AMALi the assumption of the transmittance term $T[h_f,h_{gc}]=1$ permitted accurate estimation of $\beta(h_{gc})$ for the height chosen just below a geometrical compression at 235m. The clearer the atmosphere and the better the knowledge of the molecular contribution to the extinction (nearby meteorological sounding) the better the $T[h_f,h_{gc}]$ estimate, i.e. the lower uncertainty of the $\beta(h_{gc})$ calculation. The error for neglecting the transmittance term varies from 0.7% for the particle extinction of $0.15\cdot10^{-4}m^{-1}$ (clean arctic air $T[h_f,h_{gc}]\approx0.993$), up to 2.8% for the particle extinction of $0.6\cdot10^{-4}m^{-1}$ (contaminated arctic air $T[h_f,h_{gc}]\approx0.972$). Hence, the error of the estimation of $\beta(h_{gc})$ near the aircraft and dependent on it β_{ref} found iteratively near ground, hardly affect the error of the backscatter retrieval itself. Due to the short range for both AMALi measurements (flight altitude <3km, $S/N_{min}\approx35$) the assumption of the constant lidar ratio does not introduce significant error (Tab.1). The accuracy of the backscatter coefficient calculated with the iterative approach is assumed to be $\Delta\beta_{part}=2.0\cdot10^{-7}m^{-1}sr^{-1}$

Arctic Air Type [5,6]	LR	$\Delta\beta\_part$ $[m^{-1}sr^{-1}]$
clean	20	$\pm 1.8 \cdot 10^{-7}$
low aerosol load	25	$\pm 0.3 \cdot 10^{-7}$
high aerosol load	30	$\pm 0.7 \cdot 10^{-7}$
polluted	35	$\pm 1.4 \cdot 10^{-7}$
0-0.6km 0.6-1.5km 1.5-2.5km	35 30 25	$\pm 0.9 \cdot 10^{-7}$

Tab.1 The sensitivity study of the backscatter coefficient error due to the assumption of wrong lidar ratio show no significant hindering of the iterative calculations when the constant lidar ratio is assumed.

4. INTERPRETATION

Operational T511/L60 ECMWF analyses of the near-surface flow fields indicated a low pressure system slowly propagating parallel to the Scandinavian mountain range north-eastward in a period of two days before 19 May 2004. On that day at 12:00 UTC the center of the low was located directly above Northern Scandinavia (Fig.2). Above the Norwegian Sea and Svalbard, the almost parallel easterly wind throughout

the lower troposphere was nearly uniform with a magnitude of $V_H \approx 8$m/s (not unusual flow [7]). Given a maximum buoyancy frequency of N=0.010/s the Froude number is $F=V_H/(N \cdot h_0) \approx 0.55 \ldots 1.6$, where h_0 is the maximum height of the orography. The square of this dimensionless number can be interpreted as ratio of the kinetic energy of an air parcel upstream of the obstacle to the potential energy it would gain when lifted to h_0 (for F<1 the parcels flow predominantly around the obstacle whereas for F>1 the flow has enough energy to pass over the mountains). Hence, the range of calculated F for h_0=0.5…1.5km explain a partial flow around and above Svalbard.

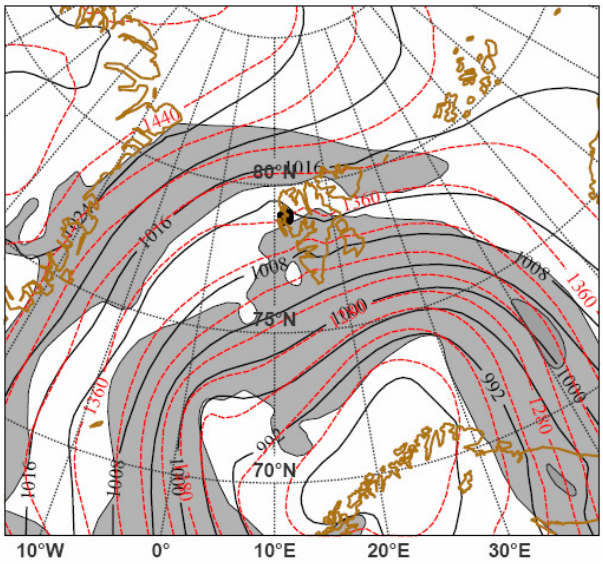

Fig.2. Mean sea level pressure (hPa; solid black lines), geopotential height (m; red dashed lines) and horizontal wind speed >10m/s (m/s; shaded, contour interval 10m/s) at 850hPa valid on 19 May 2004 12:00 UTC.

The characteristic Foehn-like area of warm air west off Svalbard and colder air surrounding it in the North and over the land with a maximum temperature difference of about 7K is well captured (Fig.3, top). Due to the adiabatic cooling of the ascending air, the area east of the largest mountains cools below 260K associated with increased values of the cloud ice and liquid water content (Fig.3, bottom); during descent the air warms and forms the observed cloud-free gap with negligible values of cloud ice and liquid water content west off Svalbard. Remarkable is the formation of a localized jet with V_H>15m/s at the northern tip of Svalbard, at around 80°N and 3-9°E, so-called corner-wind, similar to the tip jets occurring at the southern tip of Greenland [8,9]. Further south in the lee of the mountain at around 79°N and 5-11°E the V_H decreases below 2m/s forming a broad wake region in the warm air. Further south the magnitude of the horizontal wind speed increases again in association with the low pressure system located over Northern Scandinavia. The vertical winds show wave-like structures with periodically changing sinking and rising obviously locked to the underlying orographic obstacles. Note that the mentioned above features (the northern jet, the wake region, and the winds associated with low pressure system in the south) correspond to the different aerosol load in backscatter ratio profiles along flight in Fig.1.

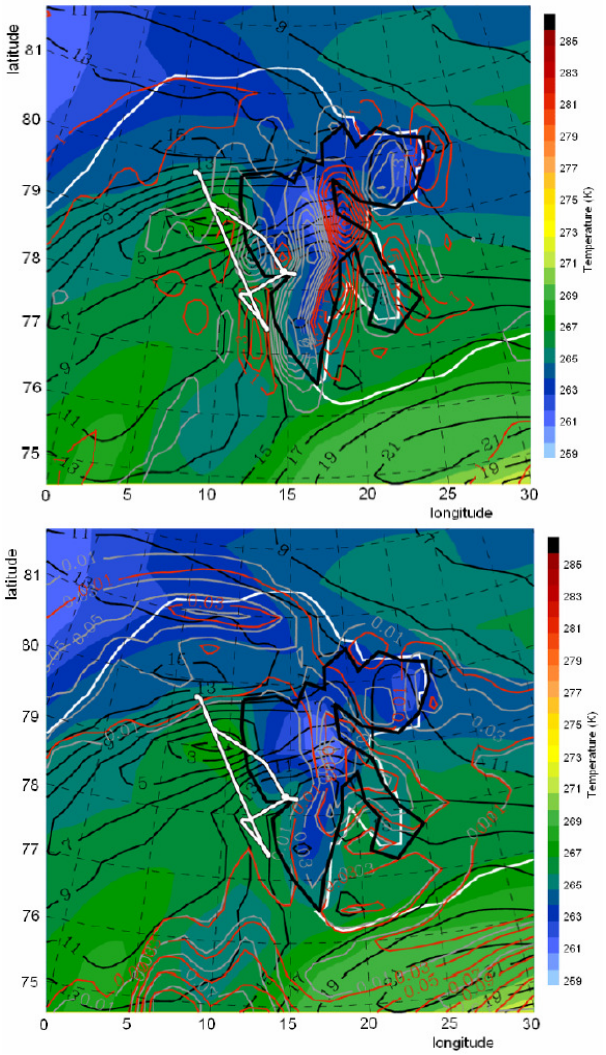

Fig.3. Horizontal cross-sections of horizontal wind speed (black solid lines; m/s), temperature (color shaded; K), top: the vertical velocity (red positive, gray negative; cm/s, bottom: cloud ice water content (red lines; gk/g) and cloud liquid water content (gray lines; gk/g). Model level 8 (~1km altitude) valid on 19 May 2004 12:00 UTC. The white solid lines mark the ice edge and corresponding Polar 2 flight path.

The meteorological conditions up- and downstream of Svalbard are characterised by means of vertical cross-sections for 30°E and 10°E, respectively (Fig.4).

At a longitude of 30°E, the isentropes indicate an inversion layer (increased thermal stability, i.e. denser contour lines) at about 0.5km altitude north of 81°N over the pack ice region. Towards south, the height of this capping inversion increases to 1…1.5km altitude; south of 77°N tilted isentropes mark the baroclinic zone associated with the low pressure system further south. There, the magnitude of the horizontal wind speed V_H is

maximum and amounts to about 22m/s. Directly upstream of Svalbard, $V_H \approx 6 \ldots 12$m/s depending on the altitude. The clouds visible in backscatter ratio in Fig.1 are realized by enhanced values of cloud ice and liquid water content upstream of Svalbard. The vertical wind speed at this upstream section is very low without any coherent structures.

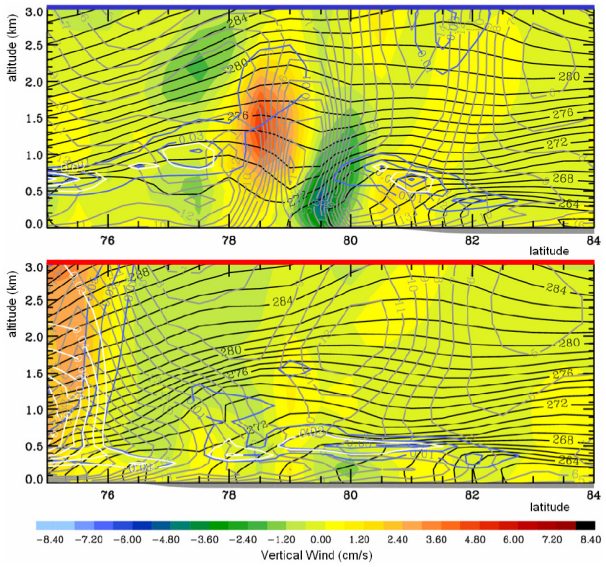

Fig.4. Vertical cross-sections of vertical wind (color shaded; cm/s), horizontal wind speed (gray solid lines; m/s), potential temperature (solid black lines; K), cloud ice water content (white lines; gk/g) and cloud liquid water content (blue lines; gk/g) along 10°E (top) and 30°E (bottom) valid on 19 May 2004 at 12:00 UTC. The grey areas below the abscissas mark correspond to the pack ice location up- and downstream of Svalbard, respectively.

In contrast, the downstream vertical cross-section at 10°E reveals pronounced up- and downdrafts between 78°N and 81°N belonging to two counter-rotating horizontal vortex tubes with axes pointing into the plane plotted in Fig.4: south of the ice edge, the northern vortex rotates anticlockwise and produces the strong downdraft at about 79°N in concert with its clockwise rotating counterpart further south. Directly north of the downdraft in the center of the northern vortex tube, the horizontal wind speed is maximum ($V_H \approx 16$m/s at about 0.4km altitude) indicating the corner-wind or tip jet as seen in Fig.3.
It is interesting to note that the isentropic surfaces in the vicinity of the ice edge are lifted significantly due to the upward motion and dropped due to the descending in the vortex. This results in a rather steep slope of isentropic surfaces along the south-north flight path of Polar 2 on this day (Fig.3). This characteristic shape of the isentropes and associated with it enhanced vertical transport of the sea salt aerosols from the rough sea in the region of the corner-wind lead to a triangularly-shaped distribution of the lidar backscatter ratio (Fig.1).

5. CONCLUSIONS

An alternated approach for the iterative backscatter coefficient retrieval using calibration by lidar signals itself was proposed and demonstrated. The results obtained with the airborne lidar AMALi were discussed with respect to the different error contribution.
The retrieved backscatter ratios on 19 May 2004 were interpreted by means of T511/L60 ECMWF operational analyses. The different boundary layer aerosol loads along flight correspond to meteorological features; the northern tip-jet, the wake region, the winds associated with low pressure system in the south.
The Svalbard orography effect on aerosol distribution will be further studied by a high-resolution numerical experiment using the non-hydrostatic model EULAG.

REFERENCES

1. Stachlewska I.S., Investigation of tropospheric arctic aerosol and mixed-phase clouds using airborne lidar technique. *PhD Thesis, University of Potsdam,* urn:nbn:de:kobv:517-opus-6984, http://opus.kobv.de/ubp/volltexte/2006/698/, 2006

2. Klett J.D., Lidar inversions with variable backscatter/extinction values. *Applied Optics* 24, 1638-1648, 1985

3. Stachlewska I.S., et al. Airborne Mobile Aerosol Lidar for measurements of arctic aerosol. *ILRC22, ESA SP-561*, 87-89, 2004

4. Arctic Study of Tropospheric Aerosol, Clouds and Radiation, http://www.awi-potsdam.de/www-pot/astar

5. Stachlewska, I.S., et al. Application of the two-stream inversion algorithm for retrieval of extinction, backscatter, and lidar ratio for clean and polluted Arctic air. *Lidar Technologies, Techniques and Measurements for Atmospheric Remote Sensing, Proceedings of SPIE*, Vol.5584, 03/1-03/8, 2005

6. d'Almeida G.A., et al. Atmospheric aerosols: Global climatology and radiative characteristics, A. *Deepak Publishing,* Virginia, 1991

7. Skeie P. and Grønås S., Strongly stratified easterly flows across Spitsbergen, *Tellus* 52A, 437-486, 2000

8. Moore G.W.K. and Renfrew I. A., Tip jets and barrier winds; A QuickSCAT climatology of high wind speed events around Geenland, *Journal of Climate* 18, 3713-3725, 2005

9. Sandvik A. D. and Furevik B. R., Case study of a costal jet at Spitsbergen. Comparison of SAR and model estimated wind. *Monthly Weather Review* 130, 1040-1051, 2002